

# The *XMM*-Large Scale Structure catalogue: X-ray sources and associated optical data. Version I

M. Pierre,<sup>1\*</sup> L. Chiappetti,<sup>2</sup> F. Pacaud,<sup>1</sup> A. Gueguen,<sup>1</sup> C. Libbrecht,<sup>1</sup> B. Altieri,<sup>3</sup> H. Aussel,<sup>1</sup> P. Gandhi,<sup>4†</sup> O. Garcet,<sup>5</sup> E. Gosset,<sup>5</sup> L. Paioro,<sup>2</sup> T. J. Ponman,<sup>6</sup> A. M. Read,<sup>7</sup> A. Refregier,<sup>1</sup> J.-L. Starck,<sup>1,8</sup> J. Surdej,<sup>5</sup> I. Valtchanov,<sup>3</sup> C. Adami,<sup>9</sup> D. Alloin,<sup>1</sup> A. Alshino,<sup>6</sup> S. Andreon,<sup>10</sup> M. Birkinshaw,<sup>11</sup> M. Bremer,<sup>11</sup> A. Detal,<sup>5</sup> P.-A. Duc,<sup>1</sup> G. Galaz,<sup>12</sup> L. Jones,<sup>6</sup> J.-P. Le Fèvre,<sup>8</sup> O. Le Fèvre,<sup>9</sup> D. Maccagni,<sup>2</sup> A. Mazure,<sup>9</sup> H. Quintana,<sup>12</sup> H. J. A. Röttgering,<sup>13</sup> P.-G. Sprimont,<sup>5</sup> C. Tasse,<sup>13</sup> G. Trinchieri<sup>2</sup> and J. P. Willis<sup>14</sup>

<sup>1</sup>Laboratoire AIM, CEA/DSM - CNRS - Université Paris Diderot, DAPNIA/Service d'Astrophysique, CEA-Saclay, F-91191 Gif-sur-Yvette Cedex, France

<sup>2</sup>INAF, IASF Milano, via Bassini 15, I-20133 Milano, Italy

<sup>3</sup>ESA, Villafranca del Castillo, Spain

<sup>4</sup>Institute of Astronomy, Madingley Road, Cambridge CB3 0HA

<sup>5</sup>Institut d'Astrophysique et de Géophysique, Université de Liège, Allée du 6 Août, 17, B5C, 4000 Sart Tilman, Belgium

<sup>6</sup>School of Physics and Astronomy, University of Birmingham, Edgbaston, Birmingham B15 2TT

<sup>7</sup>Department of Physics and Astronomy, University of Leicester, Leicester LE1 7RH

<sup>8</sup>DAPNIA/SEDI CEA Saclay, 91191 Gif-sur-Yvette Cedex, France

<sup>9</sup>Laboratoire d'Astrophysique de Marseille, France

<sup>10</sup>INAF, Osservatorio Astronomico di Brera, Milan, Italy

<sup>11</sup>Department of Physics, University of Bristol, Tyndall Avenue, Bristol BS8 1TL

<sup>12</sup>Departamento de Astronomía y Astrofísica, Pontificia Universidad Católica de Chile, Santiago, Chile

<sup>13</sup>Leiden Observatory, PO Box 9513, 2300 RA Leiden, the Netherlands

<sup>14</sup>Department of Physics and Astronomy, University of Victoria, Elliot Building, 3800 Finnerty Road, Victoria, BC V8P 1A1, Canada

Accepted 2007 August 15. Received 2007 June 20; in original form 2007 February 5

## ABSTRACT

Following the presentation of the *XMM*-Large Scale Structure (*XMM*-LSS) survey X-ray source detection package by Pacaud et al., we provide the source lists for the first surveyed 5.5 deg<sup>2</sup>. The catalogues pertain to the [0.5–2] and [2–10] keV bands and contain in total 3385 point-like or extended sources above a detection likelihood of 15 in either band. The agreement with deep log *N*–log *S* is excellent. The main parameters considered are position, count rate, source extent with associated likelihood values. A set of additional quantities such as astrometric corrections and fluxes are further calculated while errors on the position and count rate are deduced from simulations. We describe the construction of the band-merged catalogue allowing rapid subsample selection and easy cross-correlation with external multiwavelength catalogues. A small optical Canada–France–Hawaii Telescope Legacy Survey multiband subset of objects are associated with each source along with an X-ray/optical overlay. We make the full X-ray images available in FITS format. The data are available at the Centre de Données de Strasbourg and, in a more extended form, at the Milan *XMM*-LSS survey data base.

**Key words:** catalogues – surveys – X-rays: general.

## 1 INTRODUCTION

The *XMM*-Large Scale Structure (*XMM*-LSS) survey has been designed to provide a well-defined statistical sample of X-ray galaxy clusters out to a redshift of unity, over a single large area, suitable for cosmological studies (Pierre et al. 2004). This requires the

\*E-mail: mpierre@cea.fr

†Present address: RIKEN Cosmic Radiation Lab, 2-1 Hirosawa, Wakoshi, Saitama 351-0198, Japan.

**Table 1.** The individual *XMM*-LSS survey pointings. Quoted exposures are effective exposures computed after filtering high background periods; pointings with too low exposures (which have been re-executed during the *XMM* AO-5) are indicated by a star and are not included in the source list presented in this paper. Shifts are the astrometric corrections:  $\Delta\text{RA}/\cos(\text{Dec.}) = \text{RA}_{\text{XMM}} - \text{RA}_{\text{correct}}$ ,  $\Delta\text{Dec.} = \text{Dec.}_{\text{XMM}} - \text{Dec.}_{\text{correct}}$  (see Section 2.3.3); the last column indicates whether the correction is based on CFHTLS W1 data (1), see Section 3, or on the USNO-A2 catalogue (2). The letter G refers to the Liège/Milan/Saclay Guaranteed Time (nominal exposure time: 20 ks) and the letter B to the observations performed during the Guest Observer phases (nominal exposure time: 10 ks).

| Internal | Field Id  | RA (J2000) | Dec. (J2000) | Exposure times (ks) |      |      | Astrometric correction     |                              | Origin |
|----------|-----------|------------|--------------|---------------------|------|------|----------------------------|------------------------------|--------|
|          | XMM ID    |            |              | MOS1                | MOS2 | pn   | $\Delta\text{RA}$ (arcsec) | $\Delta\text{Dec.}$ (arcsec) |        |
| G01      | 112680101 | 02:27:25.4 | -04:11:06.4  | 24.6                | 25.3 | 21.4 | -1.60                      | +0.53                        | 1      |
| G02      | 112680201 | 02:25:54.2 | -04:09:05.6  | 10.1                | 9.7  | 6.7  | -1.07                      | +0.00                        | 1      |
| G03      | 112680301 | 02:24:45.6 | -04:11:00.8  | 21.8                | 21.7 | 17.3 | -1.07                      | +1.07                        | 1      |
| G04      | 109520101 | 02:23:25.3 | -04:11:07.6  | 25.5                | 25.8 | 19.5 | -1.60                      | +0.53                        | 1      |
| G05      | 112680401 | 02:28:05.1 | -04:31:08.1  | 23.5                | 23.9 | 12.5 | -1.07                      | +1.07                        | 1      |
| G06      | 112681301 | 02:26:34.4 | -04:29:00.8  | 16.4                | 16.6 | 10.5 | -0.53                      | +0.53                        | 1      |
| G07      | 112681001 | 02:25:25.3 | -04:31:07.1  | 22.5                | 25.1 | 18.6 | -0.53                      | +0.00                        | 1      |
| G08      | 112680501 | 02:23:54.6 | -04:29:00.1  | 21.2                | 21.3 | 15.9 | +0.00                      | +1.07                        | 1      |
| G09      | 109520601 | 02:22:45.2 | -04:31:11.1  | 22.5                | 22.7 | 16.4 | +0.00                      | +0.53                        | 1      |
| G10      | 109520201 | 02:27:25.4 | -04:51:04.4  | 24.7                | 24.6 | 18.5 | -1.07                      | +1.07                        | 1      |
| G11      | 109520301 | 02:26:05.1 | -04:51:06.1  | 21.7                | 21.8 | 16.1 | -1.06                      | +0.53                        | 1      |
| G12*     | 109520401 | 02:24:45.4 | -04:51:11.2  | Not used            |      |      | -0.54                      | +0.53                        | 1      |
| G13      | 109520501 | 02:23:13.1 | -04:49:03.1  | 23.6                | 23.9 | 17.8 | -2.67                      | -0.53                        | 1      |
| G14      | 112680801 | 02:22:04.1 | -04:51:09.7  | 14.4                | 14.1 | 8.3  | +1.06                      | +0.53                        | 1      |
| G15      | 111110101 | 02:27:54.1 | -05:09:02.3  | 20.8                | 21.8 | 14.0 | -2.67                      | +0.00                        | 1      |
| G16a*    | 111110201 | 02:26:34.2 | -05:09:03.1  | Not used            |      |      | -1.60                      | +0.53                        | 1      |
| G16b     | 111110701 | 02:26:35.2 | -05:08:46.6  | 11.9                | 11.9 | 11.5 | +0.00                      | +0.53                        | 1      |
| G17      | 111110301 | 02:25:14.3 | -05:09:08.4  | 22.4                | 22.2 | 17.5 | -2.67                      | -0.53                        | 1      |
| G18      | 111110401 | 02:23:54.1 | -05:09:09.7  | 27.7                | 28.0 | 19.2 | -2.67                      | +0.00                        | 1      |
| G19      | 111110501 | 02:22:34.0 | -05:09:02.1  | 23.2                | 23.8 | 16.8 | -2.67                      | +0.00                        | 1      |
| B01      | 037980101 | 02:22:45.5 | -03:50:58.8  | 14.1                | 14.2 | 8.3  | -2.13                      | +0.00                        | 1      |
| B02      | 037980201 | 02:24:05.6 | -03:51:00.0  | 13.2                | 13.2 | 7.8  | -2.13                      | +0.00                        | 1      |
| B03      | 037980301 | 02:25:25.7 | -03:50:59.2  | 13.3                | 13.0 | 7.9  | -1.07                      | +0.53                        | 1      |
| B04*     | 037980401 | 02:26:45.4 | -03:51:00.1  | Not used            |      |      | -1.07                      | +0.53                        | 1      |
| B05      | 037980501 | 02:28:05.4 | -03:51:00.5  | 15.7                | 15.7 | 10.5 | -0.53                      | +1.06                        | 1      |
| B06      | 037980601 | 02:22:05.6 | -03:31:00.2  | 13.2                | 13.2 | 7.7  | -1.60                      | +0.53                        | 2      |
| B07      | 037980701 | 02:23:25.7 | -03:30:56.7  | 12.3                | 12.3 | 6.9  | -3.73                      | +0.00                        | 2      |
| B08      | 037980801 | 02:24:34.3 | -03:29:05.1  | 10.6                | 11.5 | 6.3  | -0.53                      | +1.07                        | 2      |
| B09      | 037980901 | 02:26:05.4 | -03:31:01.1  | 13.9                | 13.8 | 8.9  | -0.54                      | +0.53                        | 2      |
| B10      | 037981001 | 02:27:14.2 | -03:28:58.7  | 13.0                | 13.2 | 8.6  | -1.07                      | +2.13                        | 2      |
| B11      | 037981101 | 02:22:34.2 | -03:09:02.5  | 12.4                | 12.3 | 7.9  | -3.20                      | +1.07                        | 2      |
| B12      | 037981201 | 02:23:54.4 | -03:09:04.1  | 11.4                | 11.3 | 7.0  | -3.20                      | +0.00                        | 2      |
| B13*     | 037981301 | 02:25:14.4 | -03:08:57.4  | Not used            |      |      | -0.53                      | +1.60                        | 2      |
| B14      | 037981401 | 02:26:34.4 | -03:08:57.6  | 12.6                | 12.5 | 6.6  | -0.53                      | +3.73                        | 2      |
| B15      | 037981501 | 02:27:54.6 | -03:08:59.3  | 11.4                | 11.5 | 8.4  | -2.13                      | +1.07                        | 2      |
| B16      | 037981601 | 02:23:14.4 | -02:48:56.3  | 12.3                | 12.7 | 7.9  | -1.60                      | +2.13                        | 2      |
| B17*     | 037981701 | 02:24:34.8 | -02:48:50.0  | Not used            |      |      | -2.67                      | +3.73                        | 2      |
| B18      | 037981801 | 02:25:55.0 | -02:48:49.1  | 16.0                | 16.2 | 11.4 | -1.07                      | +2.13                        | 2      |
| B19      | 037981901 | 02:27:14.9 | -02:48:49.5  | 13.1                | 13.1 | 8.7  | -1.07                      | +2.13                        | 2      |
| B20      | 037982001 | 02:20:34.8 | -04:48:46.3  | 16.1                | 16.8 | 11.7 | -1.60                      | -0.53                        | 1      |
| B21      | 037982101 | 02:21:14.9 | -04:28:45.9  | 15.6                | 15.6 | 9.9  | -2.13                      | +0.53                        | 1      |
| B22*     | 037982201 | 02:22:05.5 | -04:11:03.9  | Not used            |      |      | +0.00                      | +0.00                        | 1      |
| B23      | 037982301 | 02:20:05.5 | -04:31:03.9  | 9.0                 | 9.6  | 6.5  | -1.07                      | +1.60                        | 1      |
| B24      | 037982401 | 02:20:45.6 | -04:11:01.2  | 18.1                | 18.2 | 10.4 | -1.07                      | +0.53                        | 1      |
| B25      | 037982501 | 02:21:25.5 | -03:51:02.4  | 11.5                | 11.9 | 6.8  | -1.07                      | -0.53                        | 1      |
| B26      | 037982601 | 02:20:34.8 | -03:28:50.4  | 14.7                | 14.6 | 8.3  | -2.13                      | +0.53                        | 2      |
| B27      | 037982701 | 02:21:14.8 | -03:08:49.1  | 16.3                | 16.2 | 10.7 | -1.60                      | +1.07                        | 2      |
| B28      | 147110101 | 02:21:55.1 | -02:49:02.4  | 11.4                | 11.6 | 9.1  | -1.60                      | +0.00                        | 2      |
| B29      | 147110201 | 02:20:35.1 | -02:49:00.1  | 10.6                | 10.6 | 8.2  | -1.60                      | +0.00                        | 2      |
| B30      | 147111301 | 02:21:15.1 | -05:09:00.7  | 12.4                | 12.5 | 9.9  | -1.07                      | +0.53                        | 1      |
| B31      | 147111401 | 02:20:36.3 | -05:28:59.5  | 10.8                | 11.0 | 8.4  | -0.53                      | +0.53                        | 1      |
| B32*     | 147111501 | 02:21:56.0 | -05:28:56.4  | Not used            |      |      | -3.20                      | +0.53                        | 1      |

ability to detect and characterize faint extended sources, in such a way as to control both the selection effects and the contamination by spurious or misclassified point-like sources. For this purpose, we have developed a dedicated X-ray image processing package,

XAMIN, which is adapted to the complex characteristics of the *XMM* focal plane (Pacaud et al. 2006). It is a two-step procedure combining wavelet multi-resolution analysis and maximum-likelihood fits, both using Poisson statistics. The package has been extensively

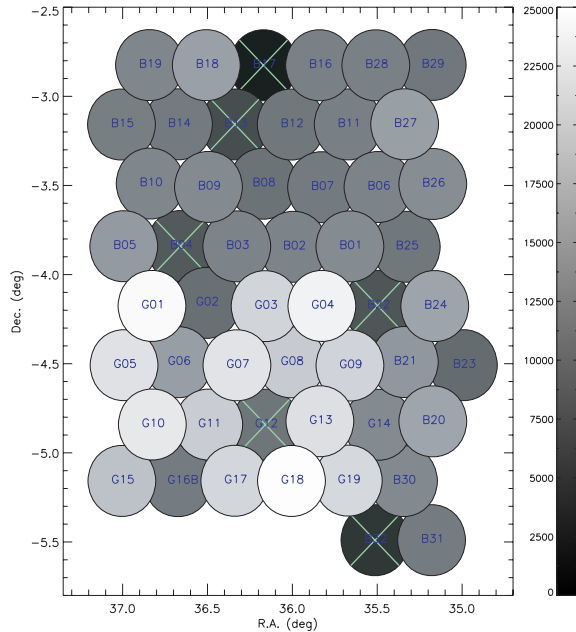


**Figure 1.** Layout of the Guaranteed Time, AO-1 and AO-2 pointings. The grey-scale indicates the effective exposure times. Pointings not included in the present release (see Table 1) are flagged by a cross. The total resulting geometrical area, taking a radius of 13 arcmin for the pointing useful radius (Section 2.3.1) amounts to  $5.5 \text{ deg}^2$ .

**Table 2.** XAMIN output parameters (Pacaud et al. 2006). See Pacaud et al. (2006) for the statistical definition of the derived likelihood values.

| Parameter     | Notes        | Content   |
|---------------|--------------|---|
| CUTRAD        |              | Size of the fitting box                                       |
| EXP           | <sup>b</sup> | Mean exposure time in the box                                 |
| GAPFLAG       | <sup>b</sup> | Distance to the nearest CCD gap                               |
| GAP_NEIGHBOUR |              | Distance to the nearest detected neighbour in the fitting box |
| EXT           |              | Best-fitting core radius                                      |
| EXT_LH        |              | Extension likelihood  |
| DET_LH        | <sup>a</sup> | Detection likelihood  |
| X_IMA, Y_IMA  | <sup>a</sup> | Best-fitting position in pixel                                |
| RA_DEC        | <sup>a</sup> | Best-fitting sky coordinates                                  |
| RATE_MOS      | <sup>a</sup> | EPIC-MOS count rate   |
| RATE_PN       | <sup>a</sup> | EPIC-pn count rate  |
| SCTS_MOS      | <sup>a</sup> | Estimated source counts in MOS1 + 2                           |
| SCTS_PN       | <sup>a</sup> | Estimated source counts in pn                                 |
| BG_MAP_MOS    | <sup>a</sup> | Background level in MOS1 + 2                                  |
| BG_MAP_PN     | <sup>a</sup> | Background level in pn  |
| PIX_DEV       | <sup>a</sup> | Distance between input/output positions                       |
| N_ITER        | <sup>a</sup> | Number of iterations in the fit                               |

Notes. <sup>a</sup>Computed for both point-like and extended profile fits. <sup>b</sup>Issued for each of the three EPIC detectors.

tested and its parameters adjusted by means of simulations, for the extended (clusters) and point-like [active galactic nucleus (AGN)] source populations; the latter representing some 95 per cent of the X-ray sources at our sensitivity of  $\sim 4 \times 10^{-15} \text{ erg s}^{-1} \text{ cm}^{-2}$  in the [0.5–2] keV band.

The first reports on cluster and AGN populations, based on the XAMIN products and an associated selection function, were published by Pierre et al. (2006) and Gandhi et al. (2006), respectively.

**Table 3.** Mean total background level (MOS1 + MS2 + pn) for the pointings included in the present catalogue, as a function of off-axis angle. Units are  $10^{-6} \text{ count s}^{-1} \text{ pixel}^{-1}$  for a pixel size of 2.5 arcsec.

| Off-axis (arcmin) | [0.5–2] keV | [2–10] keV |
|-------------------|-------------|------------|
| 0–5               | 7.1         | 12.7       |
| 5–10              | 6.3         | 12.4       |
| 10–13             | 5.8         | 12.2       |

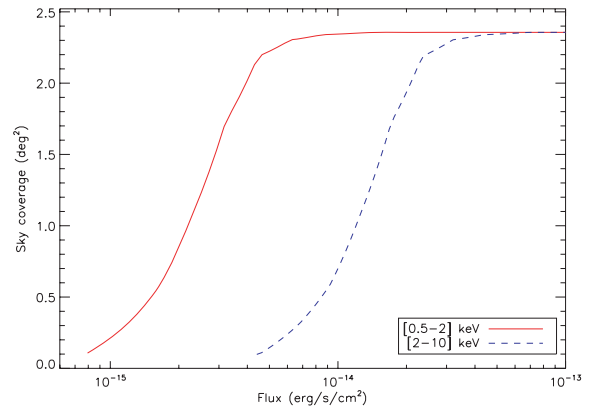


**Figure 2.** Sky coverage for the [0.5–2] and [2–10] keV bands corresponding to 27 pointings of 10 ks. The curve in the soft band is derived from extensive simulations of point sources and includes only sources having a detection likelihood  $> 15$  within off-axis distances less than 10 arcmin. The hard curve is scaled from the soft one on the basis of an equivalent S/N, using adequate background, vignetting and PSF characteristics.

The guaranteed time pointings (G fields in Table 1) were previously analysed with an independent, more traditional pipeline analogous to the one used for the HELLAS2XMM survey (Baldi et al. 2002), as described in Chiappetti et al. (2005), providing also the standard reference for the Milan XMM-LSS survey data base.

The XMM-LSS survey, located around  $2^{\text{h}}30^{\text{m}}, -5^{\circ}$ , is associated in the optical with the Wide Synoptic component of the Canada–France–Hawaii Telescope Legacy Survey<sup>1</sup> (CFHTLS – W1).

In this paper, we present the source lists obtained for the first 45 XMM-LSS survey pointings processed by XAMIN along with the relevant information on the catalogues (Section 2) as well as the X-ray images (Section 3.1). Section 3.2 describes the associated optical data that we make publicly available. The online facilities and plans for future releases are presented in the last two sections.

## 2 THE X-RAY SOURCE LISTS

### 2.1 List of available pointings

The XMM-LSS survey pointings pertaining to the Guaranteed Time, AO-1 and AO-2 periods are listed in Table 1 and displayed in Fig. 1. The raw X-ray observation data files (ODFs) were reduced using the standard XMM Science Analysis System (XMMSAS, v6.1) tasks EMCHAIN and EPCHAIN for the MOS and pn detectors, respectively. High-background periods, related to soft protons, were excluded

<sup>1</sup> <http://cfht.hawaii.edu/Science/CFHTLS/>.

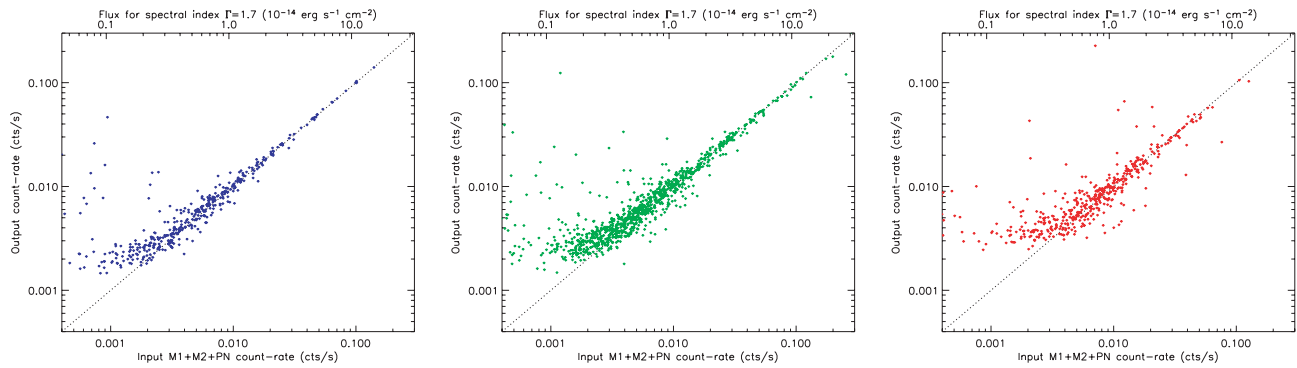


**Figure 3.** Photometric accuracy for three ranges of off-axis values from 10-ks simulated images in the soft band: 0–5, 5–10 and 10–13 arcmin. ‘Count-rate’ is the measured MOS1 + MOS2 + pn rate, normalized to the on-axis value.

from the event lists following the procedure outlined by Pratt & Arnaud (2002). The resulting light curves were visually inspected. After this operation, a number of pointings appeared to be not usable for the purpose of the *XMM*-LSS survey (too-low effective exposure times) and, consequently, are not included in the present version of the catalogue. The fields in question were re-observed during AO-5 (2006 July–2007 January) and will be published in a subsequent data release.

## 2.2 Processing and XAMIN output source parameters

Photon images in different energy bands are then created with a scale of  $2.5 \text{ arcsec pixel}^{-1}$ . Images from the three detectors (pn, MOS1, MOS2), pertaining to the same band, are co-added. The resulting image is in turn filtered in wavelet space<sup>2</sup> to remove the noise at a given significance level and subsequently scanned by a source detection algorithm set to a low threshold to obtain a primary source list. Detailed properties of each detected source are further assessed from the individual photon images using XAMIN, a maximum-likelihood profile-fitting procedure<sup>3</sup> designed for the *XMM*-LSS survey. The specific goal of this second pass is to monitor in a clean and systematic way the characterization of extended X-ray sources and associated selection effects. The principle and performances of XAMIN, for extended and point-like sources, are described in detail by Pacaud et al. (2006) and we recall here the main lines of the procedure. Basically, for each source, two spatial emission models convolved by the *XMM* point spread function (PSF) are tested: (pnt) a point source and (ext) a  $\beta$ -profile assuming a constant slope of  $2/3$ . The main parameters returned are the position and the fitted count rates and, for model ext, the best estimate of the core radius of the  $\beta$ -model. Further, for each model, the likelihood<sup>4</sup> of the source is computed, as well as the likelihood of the extension for model ext. The fits are simultaneously performed on the pn and on the MOS1 + MOS2 sum images only requiring the source centre to be the same in both images.<sup>5</sup> The procedure takes into account all main technical characteristics such as: the blurring of the PSF and

the vignetting as a function of off-axis angle and photon energy, the gaps between the CCD of the pn and MOS arrays, and the various background contributions. Results of the ext fit allow us to define two classes of extended objects in the XAMIN parameter space: the C1 and C2 classes (see Section 2.3.4). Table 2 summarizes the output parameters of the pipeline. Table 3 provides the background level, averaged over all pointings included in the present catalogue. The measurements were performed on the X-ray images (obtained after removing bad time intervals) by masking the detected source regions, for three ranges of an off-axis distance. We recall that the background consists of two components: (1) the cosmic background which is affected by the vignetting and (2) the particle background, which is significant at high energy and not affected by the vignetting. As a rule of thumb, a point-like source detected with 15 net photons in any of the three rings shows a signal-to-noise ratio ( $S/N$ ) of  $\sim 3.6$  and  $3.3$  for the [0.5–2] and [2–10] keV bands, respectively (when considering a circular aperture having a radius of 10 arcsec).

## 2.3 Source list description

In this paper, we present the source lists for two bands, [0.5–2] and [2–10] keV, named B and CD, respectively. Tables 4 and 5 display the parameters we make available: in addition to the XAMIN output, a number of parameters are a posteriori calculated in order to facilitate the interpretation of the data set. In its present state, XAMIN does not perform error calculations. Mean statistical errors were estimated by means of extensive simulations. Pacaud et al. (2006) presented a detailed account of uncertainty estimates for the extended sources (count rate and core radius). In this paper, further error information is provided for the point-source population; we note that only the first two digits are to be considered significant for the count rate and for the core radius as well as for the derived quantities.

### 2.3.1 Thresholds

XAMIN processes sources only out to an off-axis distance of 13 arcmin by applying a detection mask centred on the mean optical axis of the three telescopes, considering in this way only sources that are visible by the three detectors. The total geometrical area of the present catalogue corresponding to the validated pointings indicated in Fig. 1 amounts to  $5.5 \text{ deg}^2$ . The present version of the B and CD band catalogues contains the extended sources identified as C1 and C2 (see Section 2.3.4) to which are added sources having a point-source detection likelihood (LH) greater than 15 (so-called *non-spurious*). As shown in Fig. 2, this ensures a 90 per cent completeness limit of  $4 \times 10^{-15} \text{ erg s}^{-1} \text{ cm}^{-2}$  in the B band within

<sup>2</sup>  $\lambda$  TROU algorithm, combined with a Poisson noise model; see Starck & Pierre (1998).

<sup>3</sup> The likelihood is computed with respect to a flat image.

<sup>4</sup> The values actually provided are the natural logarithm of the likelihoods but, to follow the widespread usage, we will call them simply ‘likelihood’ throughout this paper. We refer to Pacaud et al. (2006, section 2.3.1) for clarification of this terminology issue.

<sup>5</sup> In the case of model ext, an additional fitting condition imposes that the core radii inferred from the pn and MOS1 + MOS2 images are the same.

**Table 4.** List of parameters provided in the public XMM-LSS survey catalogue. All are available at the XMM-LSS survey Milan data base in separate tables XLSSB for the soft band and XLSSCD for the hard band (the column name has an appropriate prefix: when there are two column names given, one with the prefix B and one with the prefix CD, only the one applicable to the given band appears in the relevant table but both may show up in the band-merged table; column names without prefix are relevant to the individual band only). The last four columns indicate respectively: (X) whether a parameter is natively computed by XAMIN; (m) whether a parameter is available also in the band-merged table; (o) whether a parameter is present in the XLSSOPT table together with those described in Table 10; and (C) whether a parameter is present in the catalogue stored at CDS.

| Column name                   | Units                                | Meaning and usage  | X | m | o | C |
|-------------------------------|--------------------------------------|--|---|---|---|---|
| Bseq or CDseq                 | –                                    | Internal sequence number (unique)  |   | X | X | X |
| Bcatname or CDcatname         | –                                    | IAU catalogue name XLSSx Jhhmss.s-ddmss, x=B or CD                                 |   | X | X | X |
| Xseq                          | –                                    | Pointer to merged entry see Table 5  |   | X | X | X |
| Xcatname                      | –                                    | Pointer to merged entry see Table 5  |   | X | X | X |
| Xfield                        | –                                    | XMM pointing 1-32 for B01-B32 1001-1019 for G01-G19                                |   | X |   |   |
| expm1                         | s                                    | MOS1 camera exposure in the band   | X |   |   |   |
| expm2                         | s                                    | MOS2 camera exposure in the band   | X |   |   |   |
| exppn                         | s                                    | pn camera exposure in the band   | X |   |   |   |
| gapm1                         | arcsec                               | MOS1 distance to nearest gap   | X |   |   |   |
| gapm2                         | arcsec                               | MOS2 distance to nearest gap   | X |   |   |   |
| gappn                         | arcsec                               | pn distance to nearest gap   | X |   |   |   |
| Bnearest or CDnearest         | arcsec                               | Distance to nearest detected neighbor  | X | X |   |   |
| Bc1c2                         | 0–1–2                                | 1 for class C1, 2 for C2, 0 for undefined  |   | X | X | X |
| CDc1c2                        | 0–1–2                                | 1 for class C1, 2 for C2, 0 for undefined  |   |   |   |   |
| Bcorerad or CDcorerad         | arcsec                               | Core radius EXT (for extended sources)   | X | X |   | X |
| Bextlike or CDextlike         | –                                    | Extension likelihood EXT_LH  | X | X |   | X |
| Bdetlik_pnt or CDdetlik_pnt   | –                                    | Detection likelihood DET_LH for pointlike fit                                      | X |   |   |   |
| Bdetlik_ext or CDdetlik_ext   | –                                    | Detection likelihood DET_LH for extended fit                                       | X |   |   |   |
| Boffaxis or CDoftaxis         | arcmin                               | off-axis angle   |   | X |   | X |
| Brawra_pnt or CDrawra_pnt     | ◦                                    | Source RA (not astrometrically corrected) for point-like fit                       | X |   |   |   |
| Brawdec_pnt or CDrawdec_pnt   | ◦                                    | Source Dec. (not astrometrically corrected) for point-like fit                     | X |   |   |   |
| Brawra_ext or CDrawra_ext     | ◦                                    | Source RA (not astrometrically corrected) for extended fit                         | X |   |   |   |
| Brawdec_ext or CDrawdec_ext   | ◦                                    | Source Dec. (not astrometrically corrected) for extended fit                       | X |   |   |   |
| Bra_pnt or CDra_pnt           | ◦                                    | Source RA (astrometrically corrected) for point-like fit                           | X |   |   |   |
| Bdec_pnt or CDdec_pnt         | ◦                                    | Source Dec. (astrometrically corrected) for point-like fit                         | X |   |   |   |
| Bra_ext or CDra_ext           | ◦                                    | Source RA (astrometrically corrected) for extended fit                             | X |   |   |   |
| Bdec_ext or CDdec_ext         | ◦                                    | Source Dec. (astrometrically corrected) for extended fit                           | X |   |   |   |
| Bposerr or CDposerr           | arcsec                               | Error on coordinates according to Table 8  |   | X |   | X |
| Bratemos_pnt or CDratemos_pnt | counts s <sup>-1</sup>               | MOS count rate for pointlike fit   | X |   |   |   |
| Bratepn_pnt or CDratepn_pnt   | counts s <sup>-1</sup>               | pn count rate for pointlike fit  | X |   |   |   |
| Bratemos_ext or CDratemos_ext | counts s <sup>-1</sup>               | MOS count rate for extended fit  | X |   |   |   |
| Bratepn_ext or CDratepn_ext   | counts s <sup>-1</sup>               | pn count rate for extended fit   | X |   |   |   |
| countmos_pnt                  | counts                               | MOS number of counts for point-like fit  | X |   |   |   |
| countpn_pnt                   | counts                               | pn number of counts for point-like fit   | X |   |   |   |
| countmos_ext                  | counts                               | MOS number of counts for extended fit  | X |   |   |   |
| countpn_ext                   | counts                               | pn number of counts for extended fit   | X |   |   |   |
| bkgmos_pnt                    | counts pixel <sup>-1</sup>           | MOS local background for point-like fit  | X |   |   |   |
| bkgpn_pnt                     | counts pixel <sup>-1</sup>           | pn local background for point-like fit   | X |   |   |   |
| bkgmos_ext                    | counts pixel <sup>-1</sup>           | MOS local background for extended fit  | X |   |   |   |
| bkgpn_ext                     | counts pixel <sup>-1</sup>           | pn local background for extended fit   | X |   |   |   |
| Bflux or CDflux               | erg cm <sup>-2</sup> s <sup>-1</sup> | source flux (undefined i.e. –1 for extended)                                       |   | X |   | X |
| Bfluxflag or CDfluxflag       | 0 to 2                               | 0 if MOS-pn difference <20 per cent, 1 between 20–50 per cent, 2 above 50 per cent |   | X |   | X |

an off-axis distance of 10 arcmin for the 10-ks pointings (beyond 10 arcmin, the sensitivity falls below 50 per cent of the value at the centre); in average, this corresponds to 85 and 70 sources per 20 and 10 ks pointing, respectively, judged to be real within the inner 13 arcmin.

### 2.3.2 Count rate and flux

XAMIN fits the MOS and pn count rates independently<sup>6</sup> (assuming that the two MOS have the same response). We performed a number

<sup>6</sup> While the source position and extent are fixed to be the same for the three detectors.

of point-source tests by simulating a set of 30 images in which the log  $N$ –log  $S$  distribution was injected. We display in Fig. 3 the full range of simulations detailing the photometric accuracy out to an off-axis distance of 13 arcmin (Pacaud et al. 2006, presented averaged performances). The Eddington bias is obvious for faint sources and increases with the off-axis distance; in particular, the photometry appears to be unreliable for a number of sources detected with a total count rate (pn + MOS1 + MOS2) between 0.002 and 0.005 count s<sup>-1</sup> at an off-axis angle of 10–13 arcmin. These sources are, however, detected with a likelihood greater than 15, indicating that they are real. They are thus left in the public source catalogue but their photometry should be handled with caution. Mean values for the photometric bias and accuracy are summarized in Table 6.

**Table 5.** List of data base parameters, as Table 4, but for the additional columns present only in the merged catalogue table XLSS. When there are two column names given, one with the prefix B and one with the prefix CD, they relate to the given band, and both show up in the band-merged table. Column names with the prefix X are relevant to merged properties.

| Column name              | Units                  | Meaning and usage   | X | m | o | C |
|--------------------------|------------------------|---|---|---|---|---|
| Xseq                     | –                      | Internal sequence number (unique)   | X | X | X |   |
| Xcatname                 | –                      | IAU catalogue name XLSS Jhhmss.s-ddmmssc, see Section 2.3.7                                     | X | X | X |   |
| Bspurious and CDspurious | 0 or 1                 | Set to 1 when soft/hard component has DET_LH < 15   |   | X |   |   |
| Bdetlike and CDdetlike   | –                      | Detection likelihood EXT_LH (pnt or ext according to source class)                              | X | X |   | X |
| Xra                      | °                      | Source RA (astrometrically corrected) (pnt or ext according to source class and in best band)   |   | X | X | X |
| Xdec                     | °                      | Source Dec. (astrometrically corrected) (pnt or ext according to source class and in best band) |   | X | X | X |
| Bra and CDra             | °                      | Source RA (astrometrically corrected) (pnt or ext according to source class)                    |   | X | X | X |
| Bdec and CDdec           | °                      | Source Dec. (astrometrically corrected) (pnt or ext according to source class)                  |   | X | X | X |
| Xbestband                | 2 or 3                 | Band with highest likelihood : 2 for B, 3 for CD  |   | X |   |   |
| Xastrocorr               | 1 or 2                 | Astrometric correction from CFHTLS (1) or USNO (2)  |   | X |   |   |
| Xmaxdist                 | arcsec                 | Distance between B and CD positions   |   | X |   |   |
| Xlink                    | –                      | Pointer to Xseq of secondary association, see Section 2.3.7                                     |   | X |   |   |
| Bratemos and CDratemos   | counts s <sup>-1</sup> | MOS count rate (pnt or ext according to source class)   | X | X |   | X |
| Bratepn and CDratepn     | counts s <sup>-1</sup> | pn count rate (pnt or ext according to source class)  | X | X |   | X |

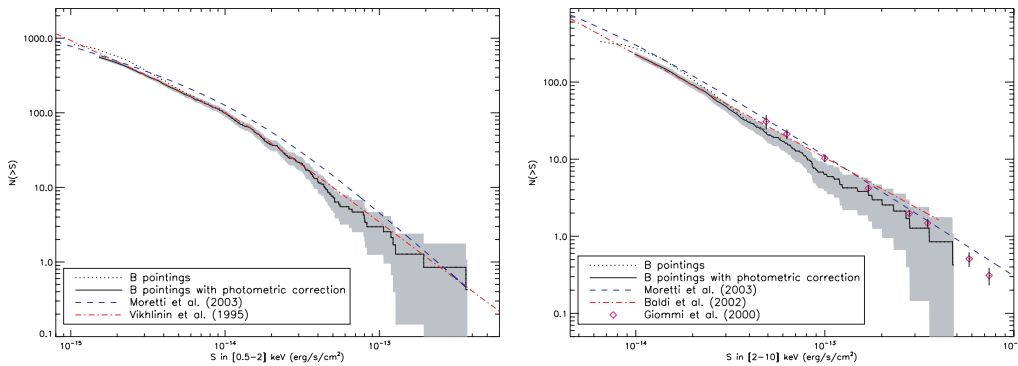


**Figure 4.** The log  $N$ –log  $S$  distributions for the soft (left-hand panel) and hard (right-hand panel) bands, involving the 27 pointings with  $\sim 10$  ks. Only sources having a detection likelihood  $> 15$  and an off-axis distance less than 10 arcmin are considered. The dotted line corresponds to the raw counts and the solid line is corrected for the Eddington bias (as conspicuous in fig. 7 of Pacaud et al. 2006). The dashed region indicates the  $1\sigma$  fluctuation level.

Count-rate values are in turn converted into fluxes assuming a standard power-law spectrum (photon index of 1.7) and the mean  $N_H$  value of the region ( $2.6 \cdot 10^{20} \text{ cm}^{-2}$ ). The energy conversion factors are given in Table 7. The observed log  $N$ –log  $S$  distributions are presented in Fig. 4; they are in good agreement with the Vikhlinin et al. (1995) (*ROSAT*), Moretti et al. (2003) (*ROSAT*, *Chandra* and *XMM*), Baldi et al. (2002) (*XMM*) and Giommi, Perri & Fiore (2000) (*BeppoSAX*) data points.

Note that the resulting pn and MOS fluxes may be quite different for some sources. In most of the cases, this is due to the fact that a part of the source is occulted by a CCD gap in one of the detectors to the point where the information is not recoverable. Such cases can be identified from the gap-related columns (Tables 2 and 4) and it is suggested to use the fitted parameters obtained from the detectors on which the source is not affected by a gap (if any). For the sake of simplicity, a single mean flux value is provided ( $[\text{FLUX}(\text{MOS}) + \text{FLUX}(\text{pn})/2]^7$ ) along with column fluxflag indicating the difference between the fluxes inferred from the MOS1 + MOS2 combination and the pn (0: less than 20 per cent; 1: between 20 and 50 per cent;

2: greater than 50 per cent). For the two single-band catalogues, the sources are roughly equally distributed between the three categories of flux quality. Fluxes assuming a thermal spectrum as well as temperature and luminosity information for the extended sources classified as C1 and C2, confirmed as clusters, can be found in the *XMM*-LSS survey cluster data base.<sup>8</sup>

### 2.3.3 Positional accuracy and astrometric corrections

The positional accuracy for the point-source population was also estimated from the simulations. Results are displayed in Fig. 5 and summarized in Table 8. We recall here that for the point-like fit, as explained by Pacaud et al. (2006), positions are fixed to those of the first pass catalogue (*SEXTRACTOR* detections on the wavelet filtered image).

In parallel, in order to compensate for possible inaccuracies in the *XMM* pointing positions, a global rigid astrometric correction was estimated using the *SAS* task *EPOSCORR*. We generated, for each *XMM* pointing, a reference X-ray list with all ‘non spurious’ point-like sources along with a reference optical list containing all CFHTLS W1 objects within 6 arcsec of the X-ray objects, being brighter than

<sup>7</sup> As the MOS count rate is about 1/3 of the pn count rate for cluster spectra, the averaged MOS flux involves a number of photons comparable to that of the pn, thus justifying the simple mean.

<sup>8</sup> <http://l3sdb.in2p3.fr:8080/l3sdb/>.

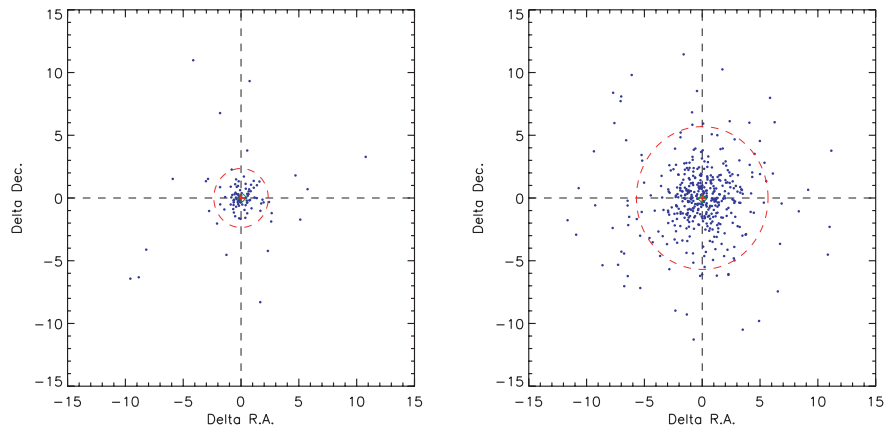


**Figure 5.** Example of positional accuracy diagrams resulting from the  $\log N$ – $\log S$  point-source simulations of 10-ks exposures in the soft band. Left-hand panel: input–output positions for the  $0 < \text{off-axis angle} < 5$  arcmin and  $\text{CR} > 0.01$  sources. Right-hand panel: input–output positions for the  $5 < \text{off-axis angle} < 10$  arcmin and  $0.002 < \text{CR} < 0.005$  sources, where CR is the measured MOS1 + MOS2 + pn count rate, normalized to the on-axis value. Axes are in units of arcseconds. The circle indicates the  $3\sigma$  rejection radius used to compute the mean positional error.

**Table 6.** Mean photometric bias ( $b$ ) and  $1\sigma$  error ( $e$ ), as a function of count-rate and off-axis distance for point sources, for each of the B and CD bands. Values (in percentile) are derived from 10 ks simulations considering sources having a detection likelihood  $> 15$  (cf. Fig. 3); below count-rates of 0.003, the output locus is degenerate and the bias is too large to estimate meaningful errors. In order to lower the flux at which the bias arises, only sources having  $\text{gap}^* > 12$  arcsec (cf. Table 4) are used for the error calculation. The true count-rate is related to the observed quantity by:  $\text{CR} = \text{CR}_{\text{obs}} [100/(b + 100) \pm e/100]$ .

| Band                                 | B      | CD     |
|--------------------------------------|--------|--------|
| Count-rate ( $\text{count s}^{-1}$ ) | $b, e$ | $b, e$ |
| $0 < \text{off-axis} < 5'$           |        |        |
| $0.003 < \text{CR} < 0.005$          | 9, 21  | 9, 22  |
| $0.005 < \text{CR} < 0.0075$         | 7, 15  | 8, 16  |
| $0.007 < \text{CR} < 0.01$           | 6, 12  | 6, 12  |
| $0.01 < \text{CR} < 0.02$            | 4, 8   | 4, 8   |
| $\text{CR} > 0.02$                   | 1, 4   | 1, 4   |
| $5 < \text{off-axis} < 10'$          |        |        |
| $0.003 < \text{CR} < 0.005$          | 10, 26 | 11, 30 |
| $0.005 < \text{CR} < 0.0075$         | 9, 19  | 9, 21  |
| $0.007 < \text{CR} < 0.01$           | 7, 15  | 5, 11  |
| $0.01 < \text{CR} < 0.02$            | 5, 10  | 2, 5   |
| $\text{CR} > 0.02$                   | 2, 5   | 1.3    |
| $10 < \text{off-axis} < 13'$         |        |        |
| $0.003 < \text{CR} < 0.005$          | –      | –      |
| $0.005 < \text{CR} < 0.0075$         | 10, 24 | 11, 29 |
| $0.007 < \text{CR} < 0.01$           | 9, 19  | 9, 21  |
| $0.01 < \text{CR} < 0.02$            | 6, 13  | 7, 14  |
| $\text{CR} > 0.02$                   | 3, 7   | 3, 7   |

$i' = 25$  and having a ‘good’ or ‘fair’ chance probability  $p < 0.03$  as defined in Section 3.3 (in the case where an X-ray source had more than one optical counterpart candidate, we retained only the one with the smallest chance probability). For the three topmost rows of XMM pointings in Fig. 1, for which the CFHTLS data are not yet processed, the optical list was made from the USNO-A2 catalogue. The reference files were fed into EPOSCORR using the parameter  $\text{maxsig} = 2$  to force removal of spurious matches. The offsets computed by EPOSCORR are plotted in Fig. 6. Offsets computed using USNO-A2 and CFHTLS objects are usually compatible within errors (with the nominal EPOSCORR errors being larger in the USNO-A2 case). The

**Table 7.** The energy conversion factors for the individual EPIC cameras and energy bands, stated in units of  $10^{-12} \text{ erg s}^{-1} \text{ cm}^{-2}$  for a rate of one  $\text{count s}^{-1}$ . A photon index power law of 1.7 and a mean  $N_{\text{H}}$  value of  $2.6 \cdot 10^{20} \text{ cm}^{-2}$  are supposed. The two MOS cameras are assumed to be identical.

| Detector | B band | CD band |
|----------|--------|---------|
| MOS      | 5.0    | 23      |
| pn       | 1.5    | 7.9     |

offsets given in Table 1 were applied to all coordinate sets for each source in the data base. The data base column XASTROCORR indicates whether the origin of the astrometric correction is the CFHTLS W1 or the USNO-A2 catalogue. Astrometrically corrected positions are used in the subsequent operations: removal of the redundant sources, source naming and cross-identification with the optical catalogue. Simulations of pairs of point sources separated by 20 arcsec show that 67 per cent of the pairs are resolved for sources having 30 photons each; all pairs being resolved when the sources contain 500 photons. As shown by Pacaud et al. (2006), a detection likelihood threshold of 15 eliminates almost all spurious detections (the corresponding contamination level is  $\sim 1$  per cent).

#### 2.3.4 Extended source classification

Pacaud et al. (2006) and Pierre et al. (2006) presented in detail the criteria for defining galaxy cluster candidates. The selection is performed in the XAMIN output parameter space obtained in the soft band. This band presents the highest S/N at any redshift for typical cluster spectra (as well as for galaxy thermal haloes) thus ensuring the highest completeness level for the extended source detection. The cluster candidate sample consists of the following two classes.

(i) The C1 class is defined such that no point sources are misclassified as extended and is described by  $\text{extent} > 5$  arcsec, likelihood of  $\text{extent} > 33$  and likelihood of detection<sup>9</sup>  $> 32$ . Note that while the C1 class is meant to be uncontaminated in terms of point-like

<sup>9</sup> For the ext fit.

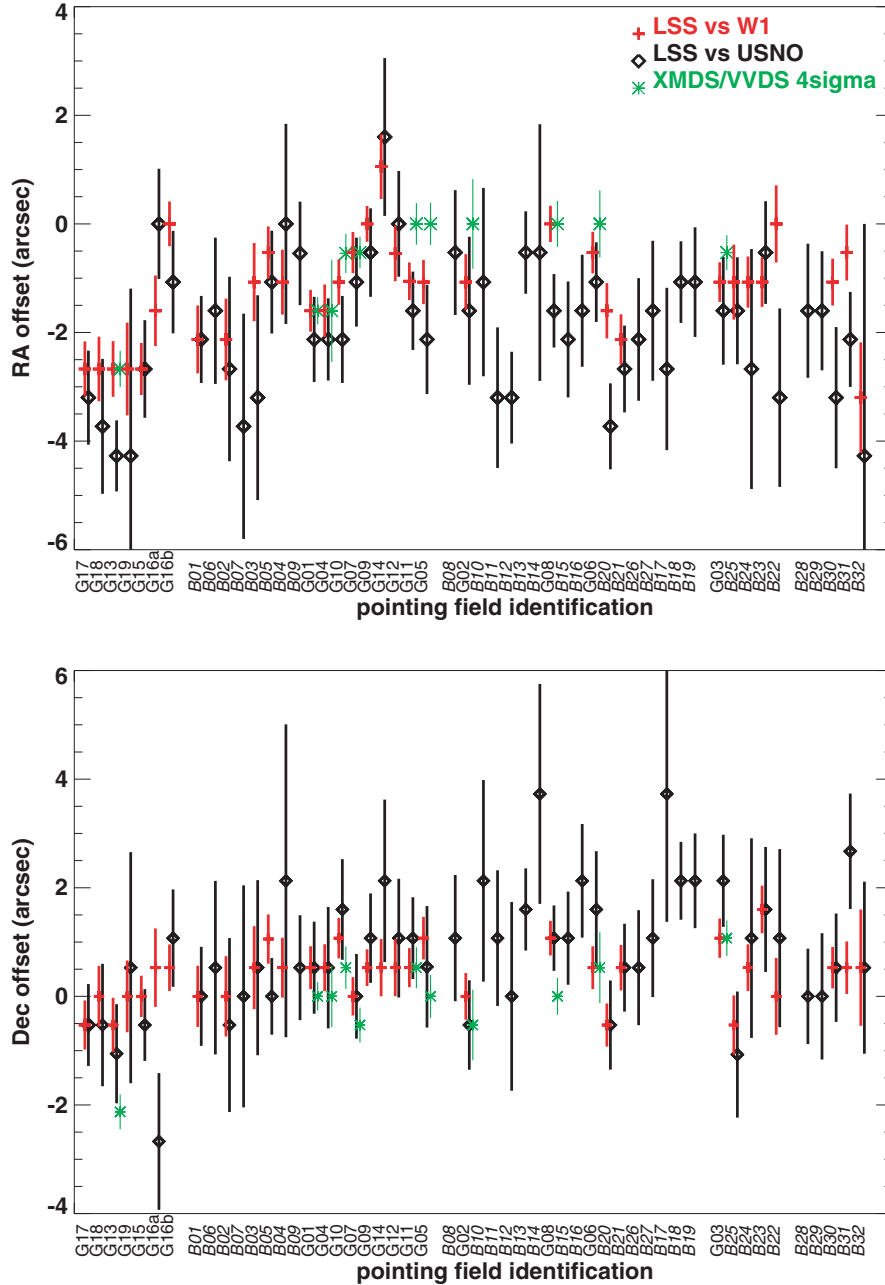


**Figure 6.** Astrometric correction offsets in RA (top panel) and Dec. (bottom panel), with nominal error bars computed by EPOSCORR. The diamonds indicate the offsets computed using the USNO-A2 catalogue, crosses those using CFHTLS W1 data, and asterisks indicate the offsets used in Chiappetti et al. (2005), when applicable. Different offsets for the same field are displaced horizontally for clarity. The x-axis gives the *XMM* pointings in chronological order of execution, with different observation ‘seasons’ separated by a blank space.

sources, it contains a few nearby galaxies whose X-ray emission is unambiguously extended (Pacaud et al., 2007).

(ii) The C2 class is described by extent  $> 5$  arcsec and  $15 < \text{likelihood of extent} < 33$  (no condition on the likelihood of detection) and typically displays a contamination rate of 50 per cent.

There are 73 C1 and C2 objects flagged in the catalogue, column Bc1c2. Note that, for the unique purpose of band merging (see below), a similar classification has been applied in the hard band. In this band, there are only 21 sources flagged as C2 and one flagged as C1, which are not detected in the soft one. A subsequent X-ray/optical inspection of these latter sources does not reveal, as expected, any

new cluster. They are mostly weak sources at extreme off-axis angle, or unresolved doubles, or cluster X-ray centroids displaced by more than 6 arcsec from the soft-band position.

### 2.3.5 Band merging

Because X-ray colours serve as a useful piece of information for numerous science studies, we provide, in addition to the individual catalogues, the two-band merged catalogue. Band merging is a delicate operation, given the rather large *XMM* PSF (full width at half-maximum  $\sim 6$  arcsec at 1 keV on axis) and its variation with energy and an off-axis angle. It may also happen that a close pair is

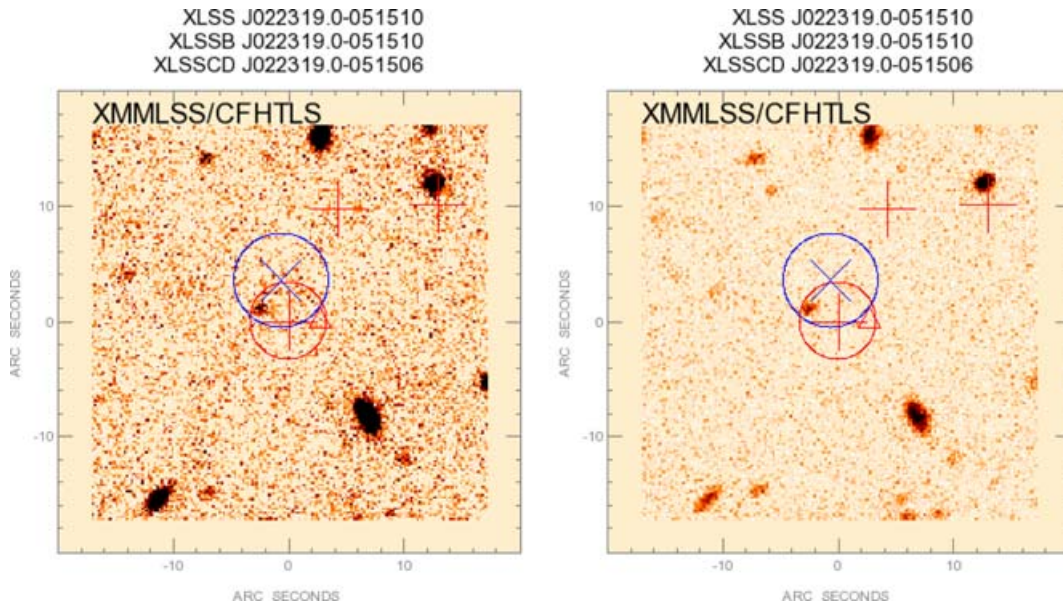


**Figure 7.** An example of postage stamp image centred on source XLSS J022319.0–051510. The CFHT *i*- and *g*-band  $40 \times 40$ -arcsec<sup>2</sup> images are shown in the left- and right-hand panels, respectively. Soft sources are indicated by a red +, and hard ones by a blue ×; all with astrometrically corrected positions. The original uncorrected position of the central source in the *best band* is indicated with a triangle of the corresponding colour. The  $2\sigma$  radius mean error circles are indicated for the central source according to the values of Table 8. All sources within the  $40 \times 40$ -arcsec<sup>2</sup> field having LH > 15 are plotted. The north is up and east is to the left-hand side.

resolved in one band only, because of too low a photon number in the other band. In order to provide the community with an efficient and reliable tool, the construction of the merged catalogue received special attention and is described below.

As an X-ray source can be detected in one or two bands and, for each band, is independently fitted by the extended and point-source models with the coordinates free, we adopt the following merging procedure. For each band, a source is classified as extended (E) if it satisfies extent > 5 arcsec and likelihood of extent > 15 (i.e. C1 or C2 class); if not, it is classified as point-like (P). Pointing per pointing, we then flag associations between the two bands within a search radius of 6 arcsec. Note that we allow associations involving spurious sources (LH < 15) at most in one band. We kept the information (rate, flux, etc.) about entries below this threshold in the merged catalogue, since it could be more useful (e.g. for upper limits) than no information at all, but we flag those cases with Bspurious = 1 or CDspurious = 1. Finally, for each soft–hard couple in the merged catalogue, we define the *best band*, that is, the band in which the detection likelihood of the source is the highest and from which the coordinates are taken. Details of the merging process are summarized in Table 9.

Starting from 2980 non-spurious sources in the soft band and 1255 non-spurious sources in the hard band, the resulting merged catalogue contains 3385 sources: out of them 50.5 per cent are detected as point-like in the soft band only, 36.3 per cent as point-like in both bands, 10.2 per cent as point-like in the hard band only; 2.1 per cent are candidate clusters of galaxies (soft band only). The remaining 0.8 per cent are mostly borderline cases (cf. end of Section 2.3.4). We note that in an extremely limited number of cases (four couples of entries) the merging process gives ambiguous results, that is, a detection in one band can be associated with two different detections in the other band. The flagging and naming of such cases is described in Section 2.3.7.

For *all* entries, we provide in the data base the distance between the positions found by XAMIN in the two energy bands (which in

most cases could be used to solve the above ambiguities). Such an interband distance, for all the cases present in both bands, except for the few ambiguities, is within 2 arcsec in 35 per cent of the cases, within 4 arcsec in 79 per cent and above 5 arcsec only in 9 per cent. These percentages change to 39, 83 and 7 per cent if we exclude detections flagged as spurious in one band. If we compare the interband distance with the combination of the position errors computed according to the prescription in Table 8, we have that in 64 per cent of the cases the interband distance is less than the  $1\sigma$  error, and in 1.4 per cent of the cases it is above  $2\sigma$ .

### 2.3.6 Removal of redundant sources

Finally, in the case of redundant objects detected in the regions where the pointings overlap, we keep in the catalogues only the detection pertaining to the pointing where the source is the closest to the optical centre (cf. columns Boffaxis, CDoffaxis in Table 4). Except for a few ambiguous cases described in Section 2.3.7, a value of 6 arcsec is found to be the adequate search radius to identify redundant detections. In this way, 280 doublets and a few triplets were identified and reduced to a single source.

### 2.3.7 Source naming

Objects in the merged catalogue are labelled following the IAU style convention, that is, XLSS Jhhmms.s-ddmms. The coordinates used in assigning the name are the ones deduced after the rigid astrometric correction, and chosen as official, that is, those for the *best band* (see Table 9).

In the individual band catalogues, the sources are assigned supplementary names, following the same standard – XLSSx JHHMMSS.S-DDMMSS – where x is B or CD and stands for the B and CD bands, respectively. In this case, the coordinates correspond to the extended (E) or point-like (P) fit in the relevant band (Table 9). As a consequence of the merging procedure (Section 2.3.5), the

**Table 8.** Positional accuracy ( $1\sigma$  error on RA or Dec.) for point sources derived from simulations of 10-ks pointings and having a detection likelihood  $>15$  (Fig. 5). Values are given for the B and CD bands, as a function of the summed measured count-rate:  $CR = MOS1 + MOS2 + pn$ . No selection is applied on the  $gap^*$  parameters (cf. Table 4) but a  $3\sigma$  rejection is performed in the calculation of the errors. Because of the strong Eddington bias for faint sources located beyond  $R > 10$  arcmin (Fig. 3), no positional errors are provided for output CR below  $0.002 \text{ count s}^{-1}$ .

| Band                                 | B              | CD             |
|--------------------------------------|----------------|----------------|
| Count-rate ( $\text{count s}^{-1}$ ) | Error (arcsec) | Error (arcsec) |
| $0 < \text{off-axis} < 5'$           |                |                |
| $0.001 < CR < 0.002$                 | 2.0            | 2.0            |
| $0.002 < CR < 0.005$                 | 1.7            | 1.7            |
| $0.005 < CR < 0.01$                  | 1.3            | 1.3            |
| $CR > 0.01$                          | 0.8            | 0.8            |
| $5 < \text{off-axis} < 10'$          |                |                |
| $0.001 < CR < 0.002$                 | 2.0            | 2.0            |
| $0.002 < CR < 0.005$                 | 1.8            | 1.9            |
| $0.005 < CR < 0.01$                  | 1.5            | 1.5            |
| $CR > 0.01$                          | 1.0            | 1.0            |
| $10 < \text{off-axis} < 13'$         |                |                |
| $0.001 < CR < 0.002$                 | –              | –              |
| $0.002 < CR < 0.005$                 | 1.9            | 2.0            |
| $0.005 < CR < 0.01$                  | 1.6            | 1.7            |
| $CR > 0.01$                          | 1.2            | 1.3            |

XLSS coordinate designation will coincide with one of the XLSSB or XLSSCD (i.e. for the *best band*).

In a limited number of cases (eight entries), a source in a band happens to be associated with two different objects in the other band. These couples of catalogue entries are flagged by a non-zero value in column `xlink`, the registered value being a pointer to the other ‘ambiguous’ entry in the couple. For those cases, the ambiguity in the XLSS name is resolved (when necessary i.e. in six out of eight cases) by the addition of a suffix: the two members of a couple will appear as XLSS JHHMMSS.S-DDMMSSa and XLSS JHHMMSS.S-DDMMSSb.

### 3 ASSOCIATED DATA PRODUCTS

#### 3.1 X-ray images

For each pointing, we make available – via the *XMM-LSS* survey data base in Milan – the following images in the FITS format. They are accessible as ‘data products’: for every source in the catalogue, a clickable link points to the images of the relevant pointings.

(i) The B and CD band photon images for the three detectors (after the event filtering).

(ii) Exposure maps for the three detectors and the two bands. All images have a pixel size of 2.5 arcsec. Note that the World Coordinate System (WCS) of the X-ray images is the one generated by the SAS; therefore, it does not take into account the astrometric correction described in Section 2.3.3 and quoted in Table 1. Consequently, when overlaying X-ray source positions exactly on the X-ray images, one should use the coordinates labelled as ‘raw’ in Table 4, although this does not make much difference for most of the sources, given the pixel size.

#### 3.2 Optical data

For each X-ray source of the merged catalogue, we provide the following.

(i) The list of optical objects within a radius of 6 arcsec around each X-ray source, extracted from the CFHTLS catalogue.<sup>10</sup> These data are available in the *XMM-LSS* survey data base in Milan only, through the XLSSOPT table. Queries on X-ray lists are allowed and return the  $u^*, g', r', i', z'$  magnitudes and further optical information derived from the Terapix merged panchromatic catalogues.

(ii) CFHTLS postage stamp images  $40 \times 40 \text{ arcsec}^2$  in the  $i$  and  $g$  bands (PNG format); in the case where a CFHTLS image is not yet processed, we provide a low-exposure CFH12K image when available. An example is shown in Fig. 7. The parameter list is given in Table 10.

#### 3.3 A few statistics

Out of our 3385 X-ray sources, 2208 have at least one optical candidate closer than 6 arcsec, 1071 fall in the area without CFHTLS coverage<sup>11</sup> (corresponding to the topmost three rows of *XMM* pointings in Fig. 1), while 106 have no optical association. The total number of associated optical objects is 6275 (the radius used here is 6 arcsec irrespective of the fact the object is extended or point-like). A total of 472 X-ray sources have a single candidate within 6 arcsec, 613 have two and the rest have more. The number of optical counterparts brighter than  $i' = 22.5$  is 1990 of which 55, 36 and 14 per cent are closer than, respectively, 3, 2 and 1 arcsec to an X-ray source (detected in any band). If we consider only the soft (B) band sources, the numbers are 1826, 56 per cent, 37 per cent and 14 per cent, respectively, while for hard (CD) band sources they are 1094, 59 per cent, 40 per cent and 17 per cent.

We further provide the distance  $d$  between the X-ray and optical positions as well as an estimate of the probability of chance coincidence

$$p = 1 - \exp[-\pi n(< m)d^2],$$

where  $n(< m)$  is the sky density of optical objects having an  $i'$  magnitude brighter than the magnitude  $m$  of the candidate counterpart, computed from the full CFHTLS W1 catalogue. Defining as ‘good’ or ‘fair’, respectively, the X-ray/optical matches having  $p < 0.01$  and  $0.01 < p < 0.03$  (as described by Chiappetti et al. 2005), we find 945 good associations and 637 fair ones. All the optical objects brighter than  $i' = 22.5$  and within 1 arcsec and 87 per cent of those within 2 arcsec have a good probability, while for a distance within 3 arcsec the percentage lowers to 69 per cent for soft sources and 73 per cent for hard sources.

### 4 SUMMARY OF ONLINE AVAILABILITY

Online data access is summarized in Table 11. Namely, we provide the following.

(i) The raw XAMIN results in individual catalogues for the B [0.5–2] keV and CD [2–10] keV bands. Only sources above a detection likelihood of 15 are made available. Redundant sources detected in overlapping regions of different pointings are removed; data from

<sup>10</sup> Currently, from the T0003 W1 field release by Terapix: <http://terapix.iap.fr/>.

<sup>11</sup> Observed, but currently still under processing.

**Table 9.** Merging decisions and definition of the *best band*. A source is defined as extended (E) in a given band if it satisfies  $\text{extent} > 5$  arcsec and likelihood of  $\text{extent} > 15$  in this band. Otherwise it is defined as point-like (P). For all sources, but the C1 clusters of galaxies, *flux* is computed from the energy conversion factors given in Table 7 using the point-source rates. For the C1 clusters, the fluxes are set to  $-1$  as the reader is addressed to the XMM-LSS survey cluster data base (spatial and spectral fitting providing accurate flux and luminosity measurements). The numbers in [] indicate the number of spurious sources encountered in the interband associations (the counterpart in and B or CD is flagged as spurious, that is, has  $\text{LH} < 15$ ).

| B band     | CD band    | Best band                         | Coordinates from | Flux in B                       | Flux in CD                      | # of sources        |
|------------|------------|-----------------------------------|------------------|---------------------------------|---------------------------------|---------------------|
| E          | Undetected | B                                 | B E_fit          | $-1$ for C1, <i>flux</i> for C2 | $-1$                            | 59                  |
| P          | Undetected | B                                 | B P_fit          | <i>flux</i>                     | $-1$                            | 1710                |
| Undetected | E          | CD                                | CD E_fit         | $-1$                            | <i>flux</i>                     | 22                  |
| Undetected | P          | CD                                | CD P_fit         | $-1$                            | <i>flux</i>                     | 347                 |
| E          | E          | Where $\text{detlik\_ext}$ is max | Best band E_fit  | $-1$ for C1, <i>flux</i> for C2 | $-1$ for C1, <i>flux</i> for C2 | 2                   |
| E          | P          | Where $\text{detlik\_ext}$ is max | Best band E_fit  | $-1$ for C1, <i>flux</i> for C2 | $-1$ for C1, <i>flux</i> for C2 | 12 [4 CD]           |
| P          | E          | Where $\text{detlik\_pnt}$ is max | Best band P_fit  | <i>flux</i>                     | <i>flux</i>                     | 5                   |
| P          | P          | Where $\text{detlik\_pnt}$ is max | Best band P_fit  | <i>flux</i>                     | <i>flux</i>                     | 1228 [36 B, 358 CD] |

**Table 10.** List of additional optical information presented as columns in the XLSSOPT table. The latter table also includes the X-ray columns marked as such in Tables 4 and 5. Therefore columns with the X, B or CD prefixes refer to X-ray parameters, those with the O prefix to optical data, and those without prefix to combined properties. The arrangement of CFHTLS W1 fields is given at <http://terapix.iap.fr/cpl/oldSite/Descart/cfhtls/cfhtlswidemosaiactargetW1.html>.

| Column name | Units      | Meaning and usage  | Terapix             |
|-------------|------------|--|---------------------|
| Oseq        | –          | Internal sequence number (unique)  | n/a                 |
| Oid         | –          | Original Terapix id in field   | id                  |
| Ofield      | –          | CFHTS field identification in form $\pm x \pm y$                               | n/a see the caption |
| Ora         | $^{\circ}$ | Right ascension of the optical candidate                                       | RA                  |
| Odec        | $^{\circ}$ | Declination of the optical candidate   | Dec.                |
| Oflag       | –          | Binary flag combining 0/1 galaxy/star, 0/4 normal/masked, 0/8 normal/saturated | flag                |
| Ou          | mag        | $u^*$ magnitude  | u                   |
| Og          | mag        | $g'$ magnitude   | g                   |
| Or_         | mag        | $r'$ magnitude   | r                   |
| Oi          | mag        | $i'$ magnitude   | i                   |
| Oz          | mag        | $z'$ magnitude   | z                   |
| Ou_e        | mag        | Error on $u^*$ magnitude   | uerr                |
| Og_e        | mag        | Error on $g'$ magnitude  | gerr                |
| Or_e        | mag        | Error on $r'$ magnitude  | rerr                |
| Oi_e        | mag        | Error on $i'$ magnitude  | ierr                |
| Oz_e        | mag        | Error on $z'$ magnitude  | zerr                |
| distance    | arcsec     | Distance from the X-ray corrected position to the optical position             | n/a                 |
| prob        | –          | Chance probability of X-ray to optical association (see the text)              | n/a                 |

**Table 11.** The XMM-LSS survey X-ray and optical data products. Individual parameter availability is given in Tables 4 and 5.

| Data sets                              | Location      | Address   |
|--|---------------|---|
| Merged XLSS catalogue, main parameters | CDS           | <a href="http://cdsweb.u-strasbg.fr/cgi-bin/qcat?J/MNRAS/vol/pag">http://cdsweb.u-strasbg.fr/cgi-bin/qcat?J/MNRAS/vol/pag</a>             |
| Single-band catalogues:                | XLSSB, XLSSCD | Milan   |
| Merged catalogue (all parameters):     | XLSS          | <a href="http://cosmos.iasf-milano.inaf.it/~lssadmin/Website/LSS/Query">http://cosmos.iasf-milano.inaf.it/~lssadmin/Website/LSS/Query</a> |
| X-ray images                           |               |   |
| Optical catalogue :                    | XLSSOPT       |   |
| Optical postage stamps                 |               |   |

the pointing where each object has the smallest off-axis angle are retained in the catalogue. In addition, fluxes assuming a power-law spectrum are provided for each point-like source.

(ii) The B–CD band merged catalogue assuming a correlation radius of 6 arcsec. This required the definition of the *best band* from which a number of parameters, such as the position, are taken and, hence, a selection of information from the single-band catalogues. Source counterparts in the other band are made available even if they have a detection likelihood below 15.

(iii) Optical: a panchromatic CFHTLS catalogue within 6 arcsec of each source of the merged catalogue as well as  $i'$ - and  $g'$ -band  $40 \times 40$ -arcsec<sup>2</sup> png images.

The *main* parameters (listed in Tables 4 and 5) of the merged X-ray catalogue are available in an electronic form at the Centre de Données de Strasbourg (CDS). The single-band and band-merged catalogues with *all* columns, as well as the associated data products (X-ray images and optical information) are accessible, with fully

interactive selection, through the *XMM*-LSS survey data base located in Milan and described by Chiappetti et al. (2005). User login details can be found in the entry web page.

## 5 FUTURE

From now on, the *XMM*-LSS survey catalogue and associated data sets will be regularly incremented following the receipt of new *XMM* and CFHTLS pointings. In parallel, *XAMIN* is being upgraded with the inclusion of information on the photon energy for the source characterization, in such a way as to better discriminate between AGN and cluster sources. When the new version is validated, we foresee reprocessing the entire data set and making it publicly available with the corresponding documentation.

## ACKNOWLEDGMENTS

The results presented here are based on observations obtained with *XMM-Newton*, an ESA science mission with instruments and contributions directly funded by ESA Member States and NASA. The optical data were obtained with MegaPrime/MegaCam, a joint project of CFHT and CEA/DAPNIA, at the Canada–France–Hawaii Telescope (CFHT) which is operated by the National Research Council (NRC) of Canada, the Institut National des Sciences de l’Univers of the Centre National de la Recherche Scientifique (CNRS) of France, and the University of Hawaii. This work is based in part on data products produced at Terapix and the Canadian Astronomy

Data Centre as part of the CFHT Legacy Survey, a collaborative project of NRC and CNRS. AG acknowledges support from Centre National d’Etudes Spatiales. The Italian members of the team acknowledge financial contribution from the contract ASI-INAF I/023/05/0. AD, OG, EG, P-GS and JS acknowledge support from the ESA PRODEX Programme ‘*XMM*-LSS’, and from the Belgian Federal Science Policy Office for their support. HQ acknowledges partial support from the FONDAP Centro de Astrofísica. PG is a Fellow of the Japan Society for the Promotion of Science.

## REFERENCES

- Baldi A., Molendi S., Comastri A., Fiore F., Matt G., Vignali C., 2002, *ApJ*, 564, 190  
 Chiappetti L. et al., 2005, *A&A*, 439, 413  
 Gandhi P. et al., 2006, *A&A*, 457, 393  
 Giommi P., Perri M., Fiore F., 2000, *A&A*, 362, 799  
 Moretti A., Campana S., Lazzati D., Tagliaferri G., 2003, *ApJ*, 588, 696  
 Pacaud F. et al., 2006, *MNRAS*, 372, 578  
 Pacaud F. et al., 2007, *MNRAS*, in press (doi: 10.1111/j.1365-2966.2007.12468.x) (arXiv:0709.1950)  
 Pierre M. et al., 2004, *J. Cosmol. Astropart. Phys.*, 9, 11  
 Pierre M. et al., 2006, *MNRAS*, 372, 591  
 Pratt G. W., Arnaud M., 2002, *A&A*, 394, 375  
 Starck J.-L., Pierre M., 1998, *A&AS*, 128, 397  
 Vikhlinin A., Forman W., Jones C., Murray S., 1995, *ApJ*, 451, 553

This paper has been typeset from a  $\text{\TeX}/\text{\LaTeX}$  file prepared by the author.